coatings

MDPI

Article

Interplay of Hydrophobic Thiol and Polar Epoxy Silicate Groups on Microstructural Development in Low-Alcohol, Crosslinked Sol–Gel Coatings for Corrosion Prevention

Shegufa Shetranjiwalla *, Andrew J. Vreugdenhil and Oliver Strong

Department of Chemistry, Inorganic Materials Research Laboratory, Trent University, 1600 West Bank Drive, Peterborough, ON K9L 0G2, Canada; avreugdenhil@trentu.ca (A.J.V.); oliverstrong@trentu.ca (O.S.)
* Correspondence: sshetranjiwalla@trentu.ca; Tel.: +1-705-748-1011 (ext. 7319)

Abstract: We have demonstrated that our patented, crosslinked, sol–gel, epoxy–thiol silicates made from the combination of (a) tetraethoxysilane (TEOS, *T*), 3-glycidoxypropyltrimethoxysilane (GPTMS, *G*), and the (b) sulfur-containing 3-mercaptopropyltrimethoxysilane (MPTMS, *S*) with TEOS in a 1:1 stoichiometric ratio form the 1:1 TGST (crosslinked epoxy and thiol silicates) coating, which can be successfully utilized for the corrosion protection of low-carbon steel. Alcohols that are a by-product of sol–gel reactions influence the network formation, crosslinking density, and formulation stability, are volatile organic contents, and are regulated in the coatings industry. To improve environmental sustainability, a series of low-alcohol (LA) formulations with TG:ST ratios of 3:1 to 1:3 was prepared to investigate the microstructural development and crosslinking reactions emerging from the interplay of the hydrophobic thiol and polar epoxy silicates induced by the low-alcohol environment. The impact on crosslinking density was characterized by Fourier Transform Infrared (FTIR), Raman, XPS, viscosity, and pot-life measurements. Low-alcohol TGST (LA(TGST)) formulations were compared, using the example of 1:1 TGST, to corresponding TGST formulations where alcohols were retained. The reduced impact of LA(TGST) formulations on global warming was quantified. The glossy and scratch-resistant LA(TGST) coatings showed 71% enhanced corrosion protection compared to the non-crosslinked hybrids.

Keywords: organic–inorganic hybrids; sol–gel; low-volatile organic content; hydrophobic coatings; anti-corrosive coatings; epoxy–thiol silicates

Citation: Shetranjiwalla, S.; Vreugdenhil, A.J.; Strong, O. Interplay of Hydrophobic Thiol and Polar Epoxy Silicate Groups on Microstructural Development in Low-Alcohol, Crosslinked Sol–Gel Coatings for Corrosion Prevention. *Coatings* **2021**, *11*, 306. https://doi.org/10.3390/coatings11030306

Academic Editor: Rita Bacelar Figueira

Received: 7 February 2021
Accepted: 5 March 2021
Published: 8 March 2021

1. Introduction

Organic–inorganic hybrid thin film coatings prepared by the sol–gel method are an attractive corrosion suppression alternative to chromate-based coatings, which are broadly recognized as being toxic to human health and the environment. The versatile chemistry of the sol–gel process [1] allows for tunable properties of coatings with improved fracture [2], abrasion, scratch and thermal resistance by incorporating inorganic components such as silicon [3], aluminum, zirconium [4], or titanium [5] under mild reaction conditions forming metal–substrate bonds. Customized nanoparticle size and porosity [6] can be achieved by controlling various formulation parameters such as pH, temperature [7], and the nature of the organic functional groups [8]. Sol–gel synthesis occurs by the polycondensation reactions that proceed with the hydrolysis and condensation of typically monomeric alkoxide sol-gel precursors [1,7] such as tetraethoxysilane (TEOS) and 3-glycidoxypropyltrimethoxysilane (GPTMS). The surface chemistry is altered as a function of the polarity of the organic component [9], transforming it into a hydrophobic or a hydrophilic surface, thereby promoting adhesion. Alcohols are released as by-products of the reaction and play an important role in the microstructural development of sol–gel derived materials. They promote the miscibility of precursors in the solvent during the synthesis, charge stabilization of intermediates, and they determine the rate of hydrolysis

of precursors [10]. In addition, alcohols transesterify hydrolyzed sol–gel species via alkoxy exchange, which is accelerated in the acidic environment and impacts particle properties under basic conditions [10]. The removal of alcohols, although easy to recycle, can alter the stability of the formulation [11], leading to phase separation or precipitation of the sol–gel colloids. Generally, alcohols are evaporated under pressure after the synthesis is complete or during coatings application. However, alcohols are volatile organic compounds (VOCs) and are highly regulated in the paints and coatings industry, prompting the development of low-VOC materials with high performance.

Coatings from GPTMS and methyltrimethoxysilane monomeric precursors that are typically used for the corrosion prevention of steel substrates have been shown to have poor adhesion [12]. Similarly, oligomeric crosslinked GPTMS and TEOS surface treatments have also failed on low-carbon steel [3]. Hybrid epoxy silane coatings grafted with different concentrations of amino silanes have shown improved performance and adhesion, but similar hybrids with thiol silanes have proved inferior [13]. In contrast, significant improvement (96%) in corrosion prevention properties has been established for polymeric (9000 g/mol) crosslinked epoxy and thiol silicates (TGST) compared to the non-crosslinked hybrids [3]. The enhanced corrosion inhibition was attributed to the covalent interactions between the epoxy silicate (TG) and thiol silicate (ST) functional groups. The alcohol content was retained during crosslinking reactions. In the present work, in order to improve the environmental sustainability of the novel coatings and understand the impact of elimination of alcohols from the formulations on the extent of crosslinking between the hydrophobic thiol and polar epoxy silicate groups and resultant changes in the coatings structure, a series of low-alcohol (LA) formulations were prepared with LA(TG):LA(ST) ratios from 3:1 to 1:3 and compared with corresponding formulations of TG and ST where alcohols were retained. The formulations were characterized by Fourier Transform Infrared (FTIR), Raman spectroscopy, and X-ray photoelectron spectroscopy (XPS), and formulation stability was monitored by viscosity and pot-life measurements. Scratch resistance was tested by pencil hardness tests using the ASTM D3363 method. The accelerated corrosion protection performance of the coatings after immersion in Dilute Harrisons Solution (DHS) was quantified using digital image analysis.

2. Materials and Methods

2.1. Materials

3-Glycidyloxypropyltrimethoxysilane (GPTMS, 98%), 3-mercaptopropyltrimethoxysilane (MPTMS, 98%), and tetraethoxysilane (TEOS, 98%) were purchased from Gelest Inc., Morrisville, PA, USA and used as received. Acetic acid and hydrochloric acid, reagent grade, was purchased from Sigma Aldrich, Oakville, Ontario, Canada and diluted with ultrapure de-ionized (DI) water with an initial resistivity of 18.2 MΩ, to form 0.05M acetic acid solution and 25% *v/v* hydrochloric acid solution, respectively. *Fluorad*™ Fluorosurfactant FC-4430, non-ionic fluoro surfactant was purchased from 3M™ and diluted to form a 0.1% *w/w* solution with ultrapure water. Low-carbon (C < 0.25%, Mn < 0.9%, P < 0.04% with remainder Fe) steel shims (8″ × 12″) were purchased from McMaster Carr (Illinois, IL, USA), and were cut into panels of 2.5″ × 1.0″, which were coated with the TGST formulations. A pencil hardness tester kit was purchased from Gardco (Paul N. Gardner Co. Inc., Florida, FL, USA).

2.2. Preparation of Sol–Gel Formulations

The low volatile organic content (VOC) formulations were prepared in three phases. First, the precursor epoxy silicate (TG) and thiol silicate (ST) formulations were prepared as reported [3]. In brief, GPTMS (0.06 mol, 14.49 mL) and TEOS (0.02 mol, 4.56 mL) were mixed in a 3:1 molar ratio. The silanes mixture was added dropwise to 21.6 mL of acidified deionized water (0.05 M acetic acid). The solution was sealed and stirred continuously (≈300 rpm) for 72 h at room temperature (RT = 22 °C). ST was prepared in another flask by mixing MPTMS (0.06 mol, 12.19 mL) and TEOS (0.02 mol, 4.56 mL)

also in a 3:1 molar ratio. The silanes mixture was added dropwise to 21.6 mL of acidified deionized water (0.05 M acetic acid). The solution was stirred continuously (≈300 rpm) for 50 min at room temperature until the mixture was clear. Second, methanol and ethanol, which are the by-products of the sol–gel reactions, were removed under reduced pressure (55 °C, ≈300 torr) from both the TG and the ST formulations after synthesis. Theoretical amounts of alcohols based on the initial 3:1 TEOS/GPTMS and MPTMS stoichiometry were removed to obtain the low-alcohol (LA) TG (coded as LA(TG)) and low-alcohol ST (coded as LA(ST)) dispersions (Scheme 1). Acidified deionized water was added as replacement of the removed alcohols to the LA(TG) and LA(ST) solutions to maintain the formulation volume, concentrations, pH, and viscosity. Third, LA(TG) was reacted with LA(ST) at room temperature for 1 h in the five stoichiometric ratios (3:1, 2:1, 1:1, 1:2, and 1:3 epoxy: thiol silicates to form homogenous LA(TGST) formulations (Scheme 1). The surfactant solution was added in a 1:2 volume ratio of surfactant solution to total sol volume and stirred for 10 min before coating the panels with the resulting formulations. The dry film thickness (DFT) was between 0.5 and 0.9 µm, which is in agreement with reported literature of similar formulations [14]. To prepare the corresponding alcohol-rich series in the five ratios described above, TG and ST formulations where alcohols were retained were reacted for 1 h at RT to form the homogenous crosslinked TGST formulations in varying stoichiometric ratios. The formulation TG:ST 1:1, which was reported earlier [3], was reprepared in this study for comparison with LA(TG):LA(ST) 1:1.

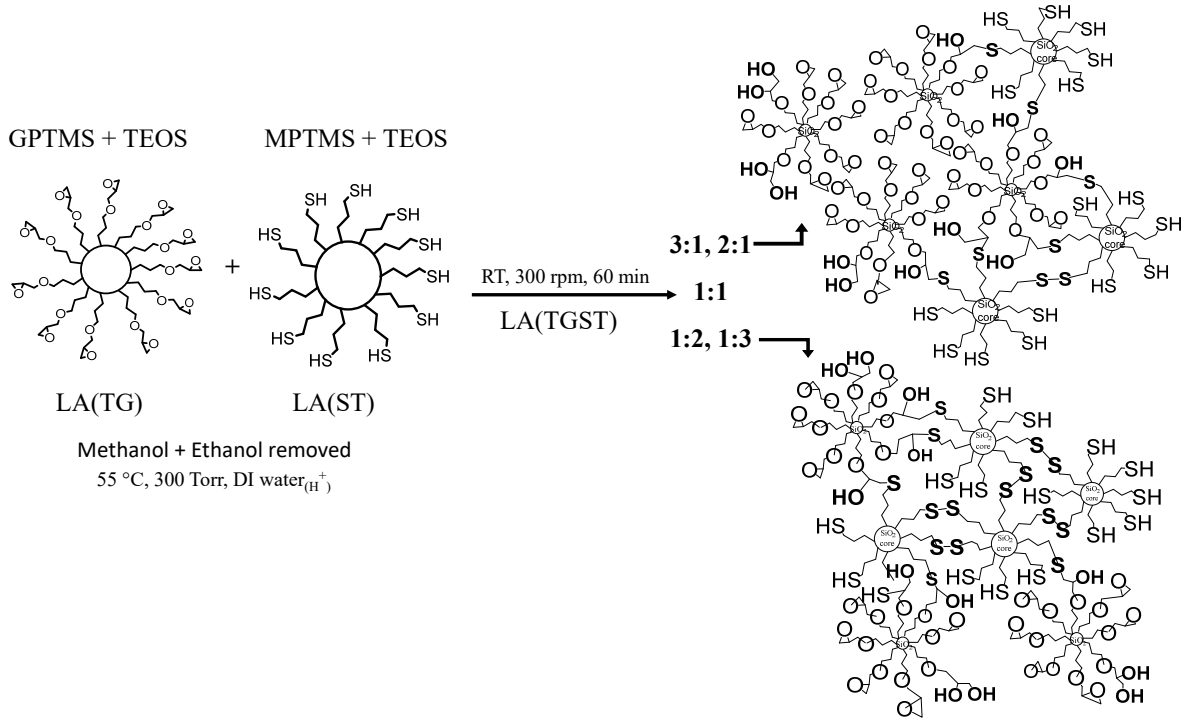

Scheme 1. Schematic microstructure and pathway for the crosslinking of low-alcohol LA(TG) and (LA)ST precursors to form the LA(TGST) system in five ratios. TG: epoxy silicate, ST: thiol silicate.

2.3. Substrate Preparation and Coatings Application

Low-carbon steel panels were cleaned by first sonicating them in acetone for 3 min followed by 3 min in a 25% hydrochloric acid bath. The panels were rinsed with distilled water between the two sonication steps to avoid contamination of the baths. To assess the corrosion protection ability of LA(TGST), six clean low-carbon steel panels were each dip-coated three times in the LA(TGST) bath. The panels were inserted for 10 s in the bath and dried for 40 s between the three applications followed by drying at room temperature in air for 24 h. All panels displayed the development of varying degrees of a dark green

layer within 1 and 5 min of coating application. A similar method was followed for panels dip-coated in a TGST bath.

2.4. Characterization

FTIR was performed on a Thermo Scientific Nicolet 380 FTIR spectrometer (Thermo Electron Scientific Instruments, LLC, Madison, WI, USA) equipped with a PIKE MIRacle™ attenuated total reflectance (ATR) system (PIKE Technologies, Madison, WI, USA). The spectra for the formulations were acquired in the scanning range of 400–4000 cm^{-1} using 64 scans at a resolution of 4 wavenumbers. All spectra were recorded at ambient temperature. The change in epoxy and thiol peak intensities were monitored after normalizing the spectra to the intensity of the peak at 2848 cm^{-1} attributed to the alkyl CH_2 C-H stretching peak.

Raman spectra for the formulations were acquired using a Renishaw inVia Raman Microscope with 633 nm excitation and an 1800 lines/mm diffraction grating. Laser power at the source was 100 mW. In total, 100 scans were co-added to achieve appropriate signal to noise in the range from 100 to 3200 cm^{-1}. The rate of change of the thiol (2580 cm^{-1}) and epoxy (1260 cm^{-1}) peak intensities was plotted by first normalizing the spectra to the intensity of the peak at 1450 cm^{-1}, which is assigned to the stretch of the alkyl group (Si-CH_2-R). Clearly discernable changes in intensity were observed at 17 h of crosslinking time, and formulations were monitored every hour after that while also continuously monitoring for gelation and precipitation.

Relative viscosity (η_{rel}) measurements using 20 mL of sample volume against acidified ultrapure water at 25 °C were conducted using a Cannon–Fenske Routine Viscometer 350 with an approximate constant (k') of 0.5 centistokes/sec with a range of 100–500 centistokes manufactured by IndusChem Lab Glass Chem Co. New Jersey. The absolute viscosity was calculated using Equation (1).

$$\text{Absolute viscosity } (\eta) \; = \; k' * \rho * t \tag{1}$$

where k' = 0.5 is the constant for the viscometer, ρ is the density of the solution, and t is the mean flow time of solution.

The XPS analyses were carried out on the coated panels with a Thermofisher Scientific K(alpha) spectrometer using a monochromatic Al Kα source (15 mA, 15 kV). The instrument work function was calibrated using sputter-cleaned Au, Ag, and Cu to determine the absolute linearity of the binding energy scale, with 83.96 eV for the Au 4f7/2 line for metallic gold, 368.21 eV for Ag 3d5/2, and 932.62 eV for the Cu 2p3/2 line of metallic copper. Survey scan analyses were carried out with 200 eV pass energy and 1 eV/step. The X-ray spot size was 400 μm (a 2:1 ellipse with the noted spot size corresponding to the major axis). High-resolution spectra were obtained with an analysis area of 300 × 700 microns and a pass energy of 20 eV. Peak fitting was done using CASA XPS (version 2.31). Electron binding energies were corrected using the carbon 1 s peak at 284.8 eV.

The corrosion resistance of LA(TGST) and TGST coated panels was monitored by immersing them in Dilute Harrison's Solution (DHS) prepared by dissolving 3.5 g $(NH_4)_2SO_4$ and 0.5 g NaCl in 1000 mL of ultrapure water with an initial resistivity of 18.2 MΩ. Six surface-treated, dry panels were first covered with waterproof adhesive tape on the edges to minimize edge effects after treatment. Three of the six samples were scribed along 3 cm to bare metal using a diamond tipped pen. The panels were placed in sealed plastic containers and then immersed in 60 mL of DHS until the first signs of corrosion were observed. Ambient dissolved oxygen levels were not monitored during the experiment; however, the typical dissolved oxygen content in NaCl solutions of this type is 6.5 ppm [15]. The rust percentage associated with the corrosion prevention performance was calculated by digital image analysis of exposed panels using the ImageJ image processing program developed at the U.S. National Institutes of Health [16].

Scratch resistance was assessed by pencil hardness tests within 48 h of coating based on the ASTM D3363 standard. Seventeen pencils of different hardnesses varying from the

softer 6B to F and harder from H to 9H (9H being hardest) were moved along the coated surface using the pencil tester at a fixed 45° angle in a 6.5 mm stroke.

Calculations for reducing the impact of volatile organic compounds (VOC) in the low-alcohol formulations were done using the International Standards Organization (ISO) metric of global warming potential (GWP) using the following equations [17–19]:

$$GWP = NC/MW_{(alcohol)}/NC_{(CO2)}/MW_{(CO2)} \quad (2)$$

where NC is the number of carbons in the molecule and MW is the molecular weight.

$$\text{Global Warming Index} = I_{(GWP)} = GWP^{*}m \quad (3)$$

where m is the mass of the emitted volatile organic compound from the prepared formulation.

3. Results and Discussion

The low-alcohol epoxy silicate LA(TG) and thiol silicate LA(ST) colloids (Scheme 1) interact with each other in two ways. First, formation of the siloxane (Si-O-Si) network by reaction of silanol groups on the surface of LA(TG) and LA(ST) colloids leads to an increase in particle size and aggregation. This directly results in an increase of the hydrophobic nature of the colloids. Second, there are the covalent interactions between LA(TG) and LA(ST) due to the simple nucleophilic epoxide ring opening by the thiol groups [11], creating new C-S bonds and introducing new hydroxyl binding sites, thus increasing the crosslinking density. This reaction constitutes a polycondensation reaction and follows the kinetics of a step growth polymerization forming a network emerging from multifunctional epoxy and crosslinking thiol groups [20]. The Si-O-Si network leads to the formation of the M-O-Si bonds with the metal substrate, facilitating strong interactions between the coating and the substrate, effectively reducing the availability of the metal surface to form metal oxides such as rust. Some of the non-polar thiol groups of LA(ST) act to provide a hydrophobic envelope which deters the diffusion of water and other polar species to the metal surface, while the other available thiol groups of LA(ST) shield the metal surface by creating a passive polymeric coating [21,22]. Finally, the formation of thiolates with the metal mitigates corrosion onset. Therefore, it is expected that a variation in the thiol concentration will (i) potentially affect the extent of epoxide ring opening by thiol groups and (ii) an increase in thiol concentration (as with LA(TGST) 1:2 and 1:3) will increase the accessibility of these groups to complement crosslinking mechanisms and further enhance the corrosion resistance properties of the LA(TGST) coatings. However, the elimination of the alcohols from the precursors before crosslinking is also expected to affect the rate of crosslinking reactions between the silica species and the thiol and epoxide groups directly impacting the microstructure, particle size, and aggregation and finally the corrosion resistance of these coatings. The LA(TGST) and the TGST coatings prepared with varying epoxy/thiol stoichiometry from 3:1 to 1:3 were fully characterized, and corrosion prevention performance was measured for both systems.

3.1. Structural Characterization

The structure of the various formulations was characterized by Raman and FTIR spectroscopy. Figure 1a shows the Raman spectra for the low-alcohol LA(TG), LA(ST), and crosslinked LA(TGST) formulations contrasted with the TG, ST, and the crosslinked TGST versions in a 1:1 stoichiometry.

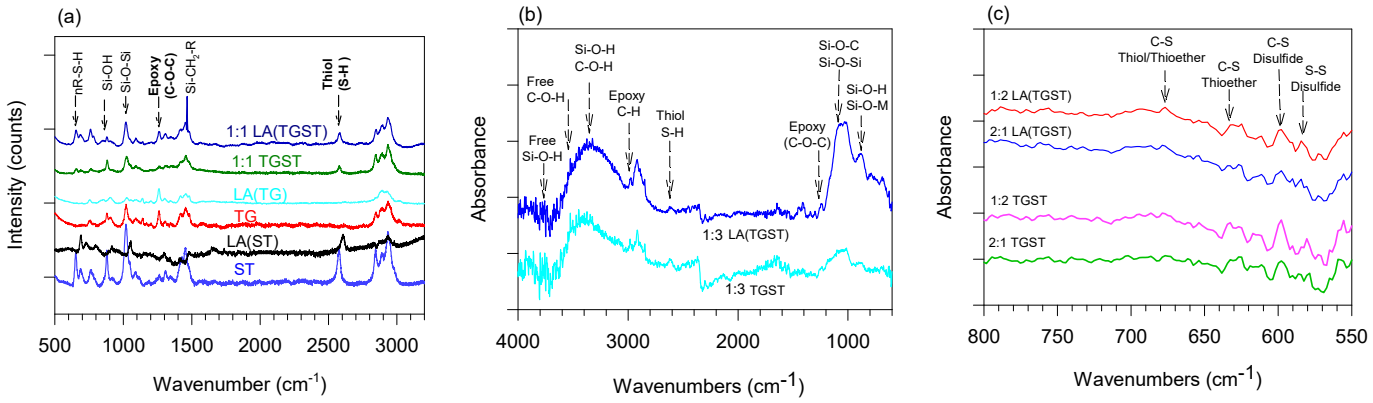

Figure 1. Structural characterization of the precursor formulations LA(TG) and LA(ST) and the hybrid LA(TGST) formulations by Raman (**a**) and Fourier Transform Infrared (FTIR) spectroscopy (**b**,**c**) contrasted with the TG, ST and the TGST hybrids.

The characteristic absorbance values for the epoxy C-O-C ring symmetric stretch (1260 cm^{-1}), thiol S-H stretch at 2580 cm^{-1}, the S-H stretch for the thiol group attached to an alky group at 652 cm^{-1}, and the peaks associated with the silica stretches namely, Si-OH (880 cm^{-1}), Si-O-Si (1020 cm^{-1}), and Si-CH_2-R (1450 cm^{-1}) (Figure 1a), confirm the formation of crosslinked colloidal silica networks from TG and ST [23]. Furthermore, the reduced intensity of the epoxy and thiol peaks in LA(TGST) and TGST formulations relative to LA(TG), TG, and LA(ST), ST indicate that the epoxy–thiol curing is extensive in both systems. In addition, interfacial interactions between TG and ST to form TGST for the 1:1 hybrid have been shown to occur immediately [3]. Figure 1b shows the FTIR spectra for the 1:3 LA(TGST) and TGST formulations that complement the structural identification by Raman spectroscopy. Characteristic peaks for the C-H of the three-membered epoxy ring (2978 cm^{-1}), C-O-C epoxy ring breathing (1248 cm^{-1}), S-H stretching vibration for the thiols groups (2615 cm^{-1}), silanol (Si-OH, 890 cm^{-1}), and Si-O-M (≈900 cm^{-1}), Si-alkoxy (Si-O-C) and siloxane (Si-O-Si) bonds at ≈1110 cm^{-1}, and the unbounded and intermolecularly bonded alcohol and silanol stretching vibrations above 3400 cm^{-1} confirm the crosslinked nature of the hybrids [3,24]. Figure 1c indicates the characteristic peak assignments for the thiol (C-S-H, 678 cm^{-1}), thioester (C-S-C, 632 cm^{-1}), the C-S (599 cm^{-1}), and S-S (580 cm^{-1}) bond vibrations associated with the disulfide (C-S-S-C) bonds in the fingerprint region [25] for the 1:2 and 2:1 ratios, respectively. The presence of all the characteristic peaks in the crosslinked low-alcohol LA(TGST) formulations confirms that the removal of alcohols did not affect the structural integrity of the formulations (Figure 1a,b). Spectra for all formulations in the fingerprint region are provided in Figure S1 in the Supporting Information.

3.2. Effect of Stoichiometric Variation on Crosslinking Density in Low-Alcohol Formulations

To investigate the impact of elimination of alcohols on the extent of crosslinking of the epoxy–thiol silicates and the sol–gel network formation for the varying ratios, Raman and IR spectroscopy of the TGST formulations was conducted to clearly elucidate the microstructural changes incurred by the LA(TGST) system when alcohols were absent. Raman spectrum for the TG:ST 1:1 formulation was measured again for this study and normalized to compare with the LA(TGST) 1:1 formulation.

Raman spectra showing the variation of the normalized intensities of epoxy and thiol peaks with change in epoxy–thiol silicate stoichiometry after completion of the crosslinking reaction (crosslinking time t = 0 h) and then at t = 20 h of curing time are shown in Figure 2a,b. Figure 2c shows the spectra for LA(TGST) ratios at 20 h. Figure 2d quantifies the extent of curing as a percentage with changing TG:ST and LA(TG):LA(ST) ratios at the different crosslinking times using the ratio of the intensity of the epoxide and thiol peaks. Table 1 shows the relative curing with the example of TGST ratios with progressing crosslinking

time. The spectral trends seen at t = 17 h crosslinking time are provided in the Supporting Information (Figure S2).

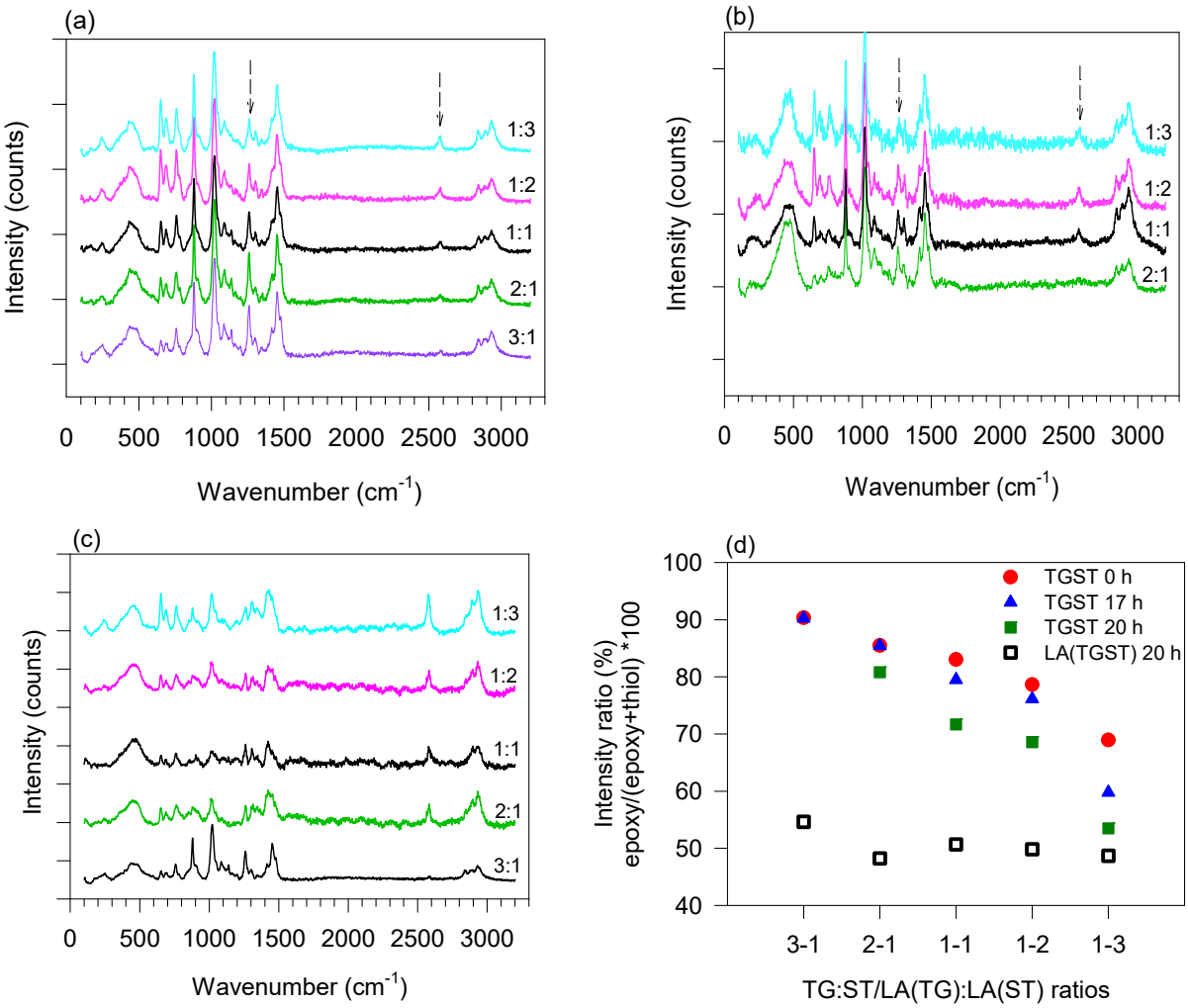

Figure 2. Raman spectra showing the variation of epoxy and thiol peaks for reaction of TGST at (**a**) 0 h, (**b**) 20 h, and for LA(TGST) at (**c**) 20 h. (**d**) Extent of curing shown by the relative intensities of epoxy and thiol moieties with increasing TG:ST/LA(TG): LA(ST) ratios at different crosslinking times.

Table 1. Variation of extent of curing in TGST formulations with changing epoxy–thiol stoichiometry.

TG:ST Ratio	Relative Epoxy–Thiol Absolute Peak Intensities			
	(a) t = 0 h	(b) t = 17 h	(c) t = 20 h	Extent of Curing with t (a Minus c)
3:1	9.335	9.260	-	Gelation
2:1	5.880	5.869	4.215	1.665
1:1	4.892	3.875	2.533	2.362
1:2	3.680	3.193	2.183	1.497
1:3	2.221	1.487	1.150	1.0703

As expected, the peak for the epoxy (C-O-C stretch, 1260 cm^{-1}, Figure 2a–c) reduced in relative intensity with decreasing TG content in the formulations from TGST 3:1 to 1:3 at all crosslinking times. Concurrently, a marked increase in the intensity of the thiol peak (S-H stretch, 2580 cm^{-1}, Figure 2a,b) was observed with increasing ST content. Interestingly, the relative intensities of the peaks for the TGST 3:1 and 2:1 ratio remain unchanged from

t = 0 h to t = 17 h (Figure 2d and Table 1), but a rapid densification and gelation was observed at t = 20 h. At 20 h, TGST 3:1 was the only formulation that had gelled completely (Table 1). Therefore, the unchanged relative intensity at t = 0 h and t = 17 h for TGST 2:1 (Table 1) indicated that the high epoxy concentration in these formulations remained in excess after completely reacting with the thiol functional groups. In TGST 2:1, which has a lower epoxy concentration, curing was evidenced by the reduced relative intensity (Figure 2d and Table 1) at t = 20 h. Therefore, it would be expected that for a similarly high concentration of thiol groups in TGST 1:3 and 1:2 formulations, a similar trend would be observed. However, a decreasing trend of relative intensities at all crosslinking times was seen, indicating higher curing (Table 1). Such a trend is attributed to two factors: (i) higher relative thiol to epoxy concentration leading to extended curing and (ii) the development of disulfide dimers. The excess concentration of sulfur containing ST in TGST 1:2 and 1:3 most likely promoted dimerization to form disulfide (S-S) bonds, which decreased the availability of functionally reactive free thiol S-H bonds in the formulation (Scheme 1). S-S dimerization in ST is consistent with the observed increase in average particle size of ST (2.4 ± 0.5) compared to TG (1.1 ± 0.6) [3]. Furthermore, TGST 1:1 showed the highest difference of relative intensity at 2.362 (Table 1), implying the presence of fewer thiol groups available to crosslink with, which can be explained by the transformation of available thiol groups to disulfide dimers in ST.

In contrast to the trends observed in the TGST system, the LA(TGST) formulations achieved a consistent (circa 50%) extent of crosslinking at t = 20 h across all ratios (Figure 2d). This indicates that irrespective of the epoxy/thiol stoichiometry, the same number of functional groups are available for crosslinking. In addition, LA(TGST) 2:1 and 1:1 have a lower thiol content than LA(TGST) 1:3, but their relative epoxy–thiol intensities are similar and are also close to that of TGST 1:3 (Figure 2d), indicating that there is considerable aggregation and dimerization in these ratios because of the removal of alcohols.

An increase in crosslinking density and disulfide formation associated with the increase in thiol content was confirmed by FTIR for all formulations. Figure 3a,b show the increase in normalized intensity for the C-H vibration of the epoxide ring with a concurrent decrease in the thiol S-H peak intensity from 1:3 to 3:1 epoxy/thiol ratios in both the TGST (Figure 3a) and LA(TGST) (Figure 3b) systems. The gradual increase was attributed to effective crosslinking between the TG and ST components. A higher peak intensity of the Si-O-H (890 cm^{-1}) and Si-O-Si peaks ($\approx$1110 cm^{-1}) for the 1:1, 1:2, and 1:3 formulations in contrast to the 3:1 and 2:1 formulations is potentially a result of enhanced hydrolysis and condensation of Si-alkoxy groups with the newly available OH groups emerging from the ring-opening of the epoxide by the higher thiol concentration (Figure 2a,b). This explains the shift to lower frequencies for the peak centers for the Si-OH and Si-O-Si peaks (shown as the dashed red arrows in Figure 3a) at 946 cm^{-1} to 890 cm^{-1} and 1110 cm^{-1} to 1050 cm^{-1} respectively from 3:1 to 1:3 ratios for TGST and LA(TGST) formulations, which is attributed to increased hydrogen bonding. The area under these peaks also corresponds to the degree of condensation between the hydrolyzed Si-O-H and the coated iron surface to form Si-O-Fe bonds. The coating–substrate covalent interactions augment the interfacial adhesion, which is an important mechanism for mitigating the onset of corrosion. Figure 3c,d show the extent of crosslinking for the TGST and the LA(TGST) systems as a function of the changes in the thiol, epoxide ring, thioester, disulfide, and alcohol bond vibration frequencies. A linear correlation was observed for all the groups associated with ST, for example, C-S-H, C-S-C, C-S-S-C, in both systems exhibiting a direct increase in crosslinking density with increasing ST stoichiometry. The linear increase in the C-S-C and C-OH peak intensities from 3:1 to 1:3 TG:ST ratios also supports the growth in extent of crosslinking arising from the increased number of thiol groups available for nucleophilic attack at the strained epoxide ring, resulting in new thioester (C-S-C) and alcohol (C-O-H) moieties (Scheme 1).

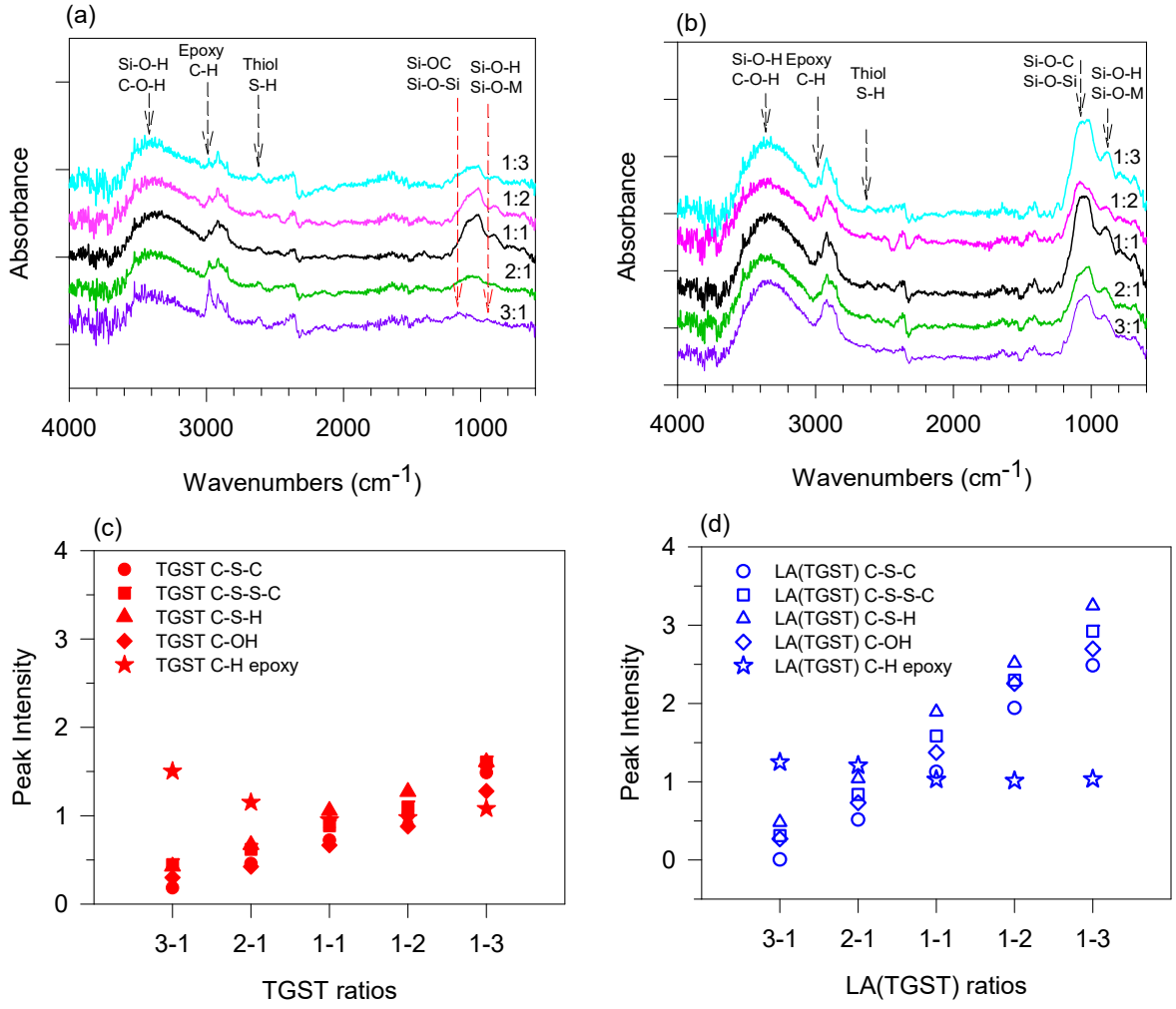

Figure 3. FTIR spectra showing the variation of epoxy and thiol peaks after reaction for (**a**) TGST and (**b**) LA(TGST) formulations. (**c**,**d**) indicate the extent of crosslinking shown by various intensities associated with the epoxy and thiol functional groups interaction with increasing TG:ST and LA(TG):LA(ST) ratios.

Interestingly, as the thiol content is increased in the formulations, disulfide content is also simultaneously elevated (C-S-S-C peak intensity in Figure 3c,d) in both systems. This is explained by the self-association of the thiol silicate particles, as illustrated in Scheme 1. An increased self-association of the more hydrophobic LA(ST) particles was also observed in the LA(TGST) system, where the alcohols were replaced with water in the formulations affecting formulation stability and increasing particle size, potentially recording increased absorbances for all peaks in Figure 3b,d. It would be expected that the C-H peak intensity of the epoxide ring would be highest for the 3:1 TG:ST ratio and would linearly decrease from 3:1 to 1:3 TG:ST, notably; however, only a marginal increase in intensity was observed from 1:1 to 1:3 TG:ST (Figure 3c). This increase in the intensity for 1:3 TGST despite improved crosslinking in high ST and LA(ST) ratios (Figure 3c,d) is attributed to the competing disulfide formation, correspondingly mitigating extensive crosslinking with available epoxy groups. In addition, although the C-OH peak intensity may be attributed to both crosslinking interactions and the formation of diols via the acid-catalyzed epoxide ring opening by water, the C-OH peak intensity was observed to be lowest for 3:1 TGST and LA(TGST) (◆ and ◇ Figure 3c,d), indicating that the ring was not extensively opened by this mechanism. In LA(TGST), independent of stoichiometry, a consistent amount of LA(TG) was consumed by LA(ST) as is indicated by the almost constant intensity of C-H epoxy peak from 3:1 to 1:3 TG:ST (Figure 3d). This implies that any expected increase in

TG:ST crosslinking was mitigated by the dimerization/self-aggregation in LA(ST) and ST colloids. The self-aggregation of thiol silicates can be explained by the absence of the charge-stabilizing presence of alcohols that were removed from the LA(TGST) formulations.

Overall, three key results can be obtained from FTIR, which are important to enhancing corrosion prevention with thiol content in the LA(TGST) and TGST formulations: (i) the growing extent of crosslinking seen in the TGST systems from 3:1 to 1:3 TG:ST ratios, in contrast to the LA(TGST) systems, indicates consistent TG:ST crosslinking irrespective of stoichiometry; (ii) extensive silanol hydrolysis and condensation is achieved in formulations with higher ST ratios; and (iii) improved adhesion of the metal substrate and the coating is obtained.

3.3. XPS Analyses

The survey scan of the coated surfaces (Figure 4a) shows the atomic percentage of key elements (C 1s, S 2p, Si 2p, O 1s) and their respective binding energies. The nitrogen and fluorine seen in the survey scan are components of the fluorosurfactant used in the coatings. The binding energies at 399.8 eV (N 1s) and 688.8 eV (F 1s) are indicative of nitrogen in amine [26] and the -CF_2-CF_2- bond [27] respectively, which are both expected from the surfactant. Figure 4b shows the deconvolution spectra of sulfur 2p for TGST 2:1 typical of spectra for all formulations. Figure 4c is plotted to reveal the correlations and extent of crosslinking between the various chemical species as a function of the LA(TG):LA(ST) and TG:ST stoichiometry and the impact of alcohol removal in the low VOC formulations.

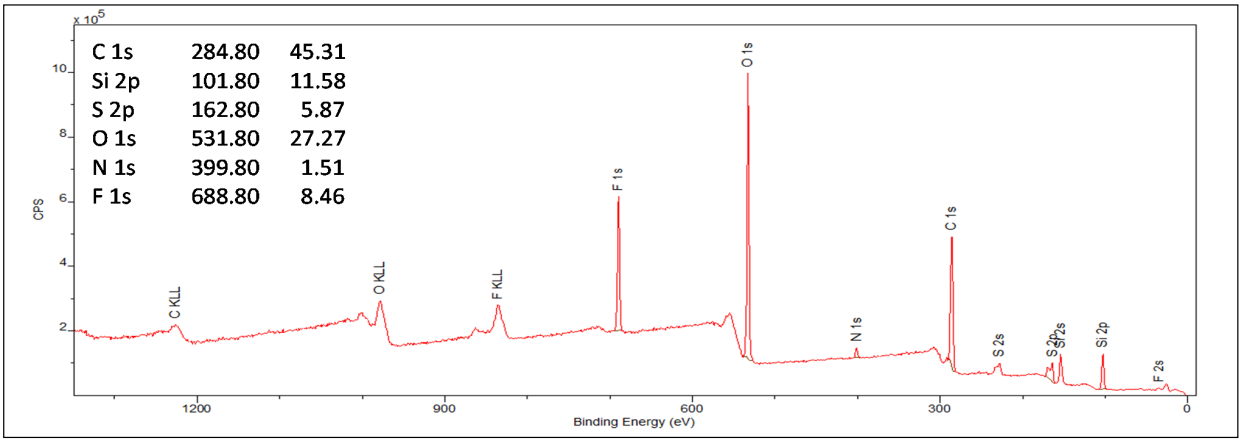

(**a**)

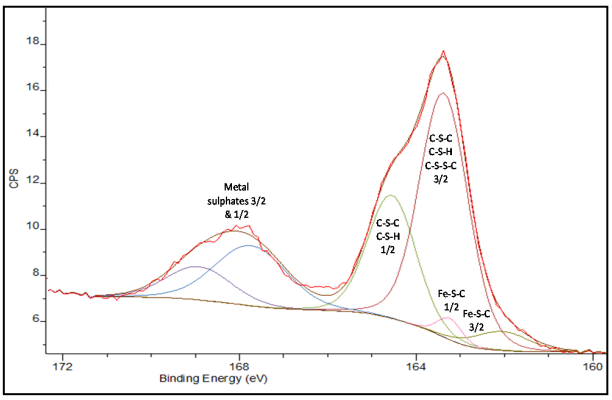

(**b**)

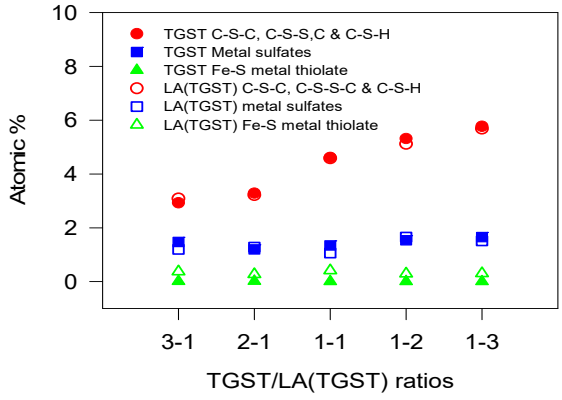

(**c**)

Figure 4. XPS spectra and correlation data for the 3:1 to 1:3 LA(TGST) and TGST ratios. (**a**) Survey scan for 1:1 TGST, (**b**) S2p peak deconvolution spectra for the various sulfur species in TGST 2:1, and (**c**) extent of crosslinking as a function of sulfur concentration.

The S 2p spectrum shown in Figure 4b was fitted by six peaks corresponding to three major species each with their S 2p 3/2 and 1/2 peak splitting at binding energies 162.2, 163.38, 163.5, 164.5, and 167.5 and 168.9 eV. The binding energy at 162.2 and 163.38 eV is associated with the 1/2 and 3/2 spin peaks of the bound thiols forming metal thiolates with iron, including a surface state contribution of the monosulfide (S^{2-}) [28–30], whereas the predominant envelope at 163.5 eV encompasses the S $2p_{3/2}$ overlap of the unbound C-S-H (thiols), C-S-C (thioester), and C-S-S-C (disulfide) groups [21,28,31,32]. The lower intensity peak at 164.5 eV is attributed to the S $2p_{\frac{1}{2}}$ binding energies for the C-S-C and C-S-H thiols groups commensurate with the spin-orbital degeneracy. Binding energies for metal sulfites and sulfates (SO_3^{2-} and SO_4^{2-}) for S 2p are observed at 167.5 eV and 168.9 eV, respectively [33,34]. The Si 2p at 102.91 eV can be fitted by a single broad peak attributed to Si-O representative of the predominant Si-O-Si network in all formulations (data not shown).

XPS analyses corroborate the results from Raman and FTIR spectroscopy. The growing extent of crosslinking between the low-alcohol and the TG and ST precursors and the increase in disulfide formation with corresponding increase in thiol content demonstrated in the infrared results is also seen in the XPS results (Figure 4c). The atomic percent of sulfur species in C-S-H, C-S-S-C, and C-S-C (●) as a function of the total atomic percent consistently increases from 2.9 atomic percent for the 3:1 to 5.7 atomic percent for the 1:3 TG:ST ratios. The C-S-H concentration in 3:1, 2:1, and 1:1 is identical and would be expected to remain unchanged at 2.9%; however, the significant increase in the C-S atomic percentage between 3.3% for 2:1 and 4.6% for 1:1 demonstrates the conversion of thiol to thioester and alkyl disulfide. This is consistent with the formation of crosslinked species and oxidation of thiols to disulfide in the presence of molecular oxygen in aqueous solutions [35]. It is expected that the enhanced epoxy–thiol crosslinking and growth of hydrophobic moieties associated with increased disulfide formation improves corrosion resistance in combination with strong substrate-coating adhesion.

The XPS information for the TGST hybrids mirrors the data for the LA(TGST) coatings (Figure 4c). Interestingly, metal sulfate formation (■, Figure 4c) is almost constant across the formulations independent of the starting concentration of thiols. This can be ascribed to the zero-order kinetics followed for the self-oxidation of thiols in the presence of atmospheric molecular oxygen. The oxidation is catalyzed by the presence of transition metal ions such as iron, although the rate of oxidation is dependent on both the pH and the nature of the transition metal [35]. Therefore, development of the green color within 1 to 5 min of air-drying coatings in all coated samples across all ratios can be attributed to the formation of iron sulfates, which is also known as green vitriol. Moreover, adhesion between the metal substrate and coating remains consistent (▲, Figure 4c) independent of stoichiometric increase in the thiol functionality. Overall, these XPS results clearly demonstrate the moieties involved in crosslinking and identify the bonds responsible for the green coloration of the coatings in the presence of atmospheric oxygen.

3.4. Formulation Stability: Viscosity and Pot-Life

Figure 5 shows the variation in viscosity for the TGST formulations at t = 0 h and t = 17 h to explore the formulation pot-life. Viscosity remained relatively unchanged with increasing TG:ST ratio immediately after reaction at t = 0 h (Figure 5). For all formulations, viscosity measurements were restricted to a maximum of t = 17 h to avoid the risk of gelation in the viscometer. The t = 17 h data point for TGST 3:1 was not measured due to signs of gelation. A significant decrease in viscosity between formulations was observed as the thiol content increased. In addition, a trend of decreasing difference in viscosity between t = 0 h and t = 17 h was observed with increasing TG:ST ratio (Figure 5). This is attributed to two main reasons: (i) the greater crosslinking between epoxy and thiol groups in formulations where the thiol content was lower but more available for reaction instead of dimerization (TGST 3:1 and 2:1) and (ii) decreasing TGST particle agglomeration. The increase in viscosity with increase in t has previously been shown to be associated with

molecular weight gain and the gradually growing aggregate size of TGST particles [3]. However, when the thiol content increases from TG:ST 1:1 to 1:3 in the formulation, ST dimerization competes with TG:ST crosslinking density, which mitigates an increase in viscosity.

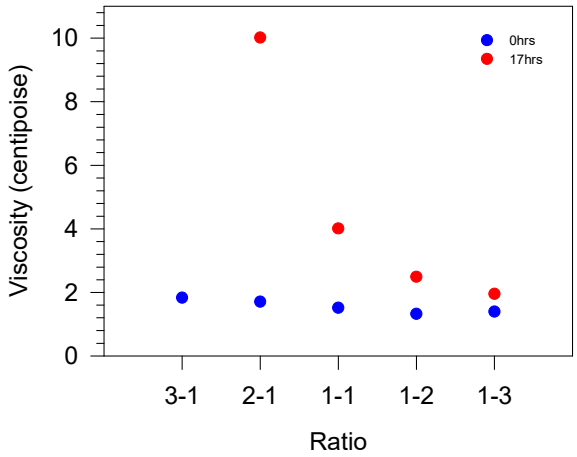

Figure 5. Change in viscosity with increasing TG:ST ratio and crosslinking time.

Pot-life was tested for the TGST system to compare with the low-alcohol LA(TGST) system to determine if the removal of alcohols from the TG and ST precursor solutions impacted the LA(TGST) formulation stability with increasing crosslinking time *t*. All solutions of TGST and LA(TGST) were clear solutions at *t* = 0 h but became progressively cloudy on standing overnight at *t* = 17 h and showed full gelation/sedimentation at *t* = 20 h (Figures S3 and S4 in the Supporting Information). Figure 6a,b shows the formulation stability of the TGST and the LA(TGST) systems at *t* = 17 h respectively. The solutions with higher TG content (3:1 and 2:1) showed signs of gel formation at *t* = 17 h and were fully gelled within 20 h. Solutions with higher ST content showed increased precipitation of TGST/ST particles in the formulation, leading to the formation of suspensions. The rate of gelation and suspension were relatively slow until *t* = 17 h but rapidly increased between *t* = 17 and 20 h (Figure S2 in the Supporting Information). The stability of formulations with respect to LA(TG): LA(ST) and TG:ST stoichiometry was observed to be 2:1, 1:1, and 1:2 greater than 3:1 and 1:3.

Figure 7a–d show the formulation stability of the precursor formulations TG, LA(TG), ST, and LA(ST). A significant difference in formulation stability between the TG and the ST dispersion and their corresponding low-alcohol precursors was observed. The TG and the low-alcohol LA(TG) formulations displayed excellent stability, maintaining their viscosity for over 30 days after preparation (Figure 7a,b). ST (where no alcohols were removed) remained stable for over 30 h under ambient conditions (Figure 7c); however, the LA(ST) formulation (Figure 7d) turned cloudy within 17 h when the alcohols were replaced with water. Although the alcohols were replaced with water to prepare a low VOC system, the thiol group that is relatively less polar than the epoxide is also less stable in a predominantly aqueous environment, thus reducing the pot-life of LA(ST) substantially. This explains the reduced stability of the LA(TGST) formulations (Figure 6b and Figure S3 in the Supporting Information) for the corresponding crosslinking times as compared to the TGST system (Figure 6a). Visibly, the LA(TGST) 1:2 and 1:3 formulations (Figure 6b) look less cloudy than their TGST counterparts at *t* = 17 h (Figure 6a) and *t* = 20 h; however, this is due to the increased sedimentation caused by the lower stability of the TGST/ST particles in the low-alcohol formulation. The bilayer in the formulation formed due to sedimentation is visible for TGST 1:2 at *t* = 20 h in Figure S3 in the Supporting Information. Expectedly, all formulations with a higher epoxy ratio (LA(TGST) and TGST 3:1, 2:1) showed gelation/sedimentation of LA(T)/ST later than the LA(TGST) and TGST 1:1, 1:2, or 1:3 formulations, which was attributed to

the lower LA(ST)/ST concentration precipitating out of the dispersions. It is of note that all formulations of the LA(TGST) and TGST systems exhibited a pot-life >15 h and were readily coated on steel panels at that time, indicating that the formulations were adequately stable over a period sufficient for commercial application of the surface treatment.

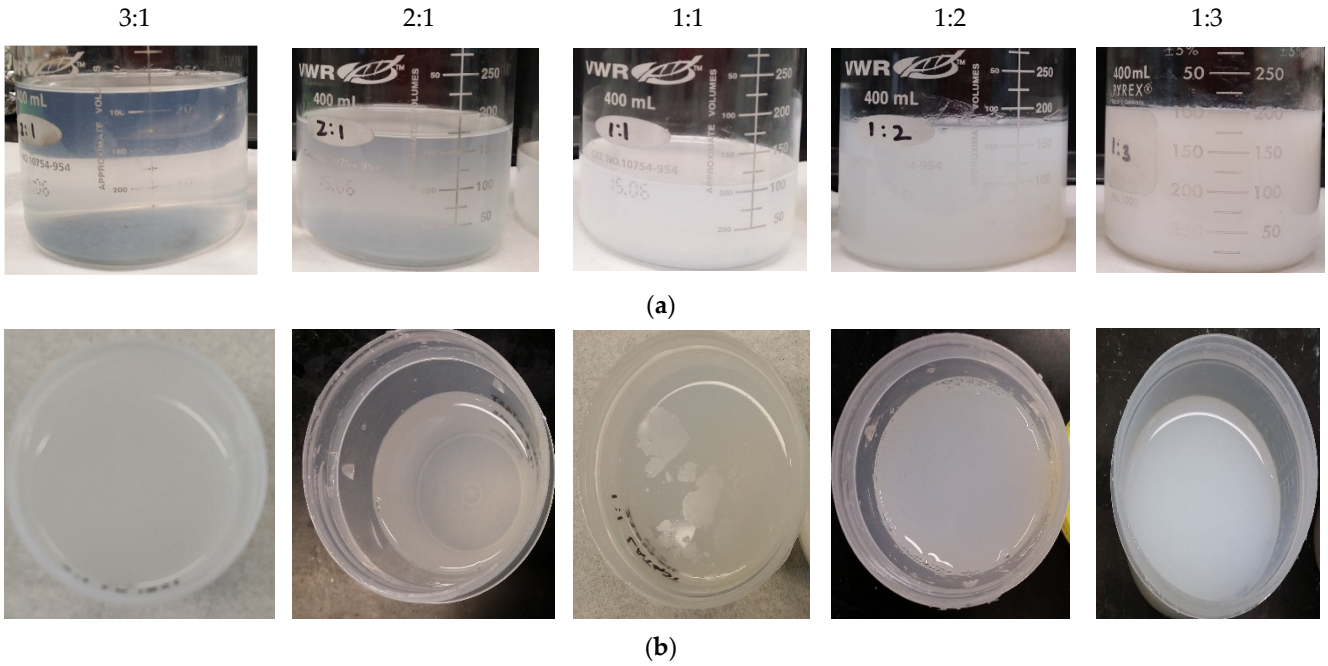

Figure 6. Pot-life for (**a**) TGST and (**b**) LA(TGST) solutions at crosslinking time t = 17 h.

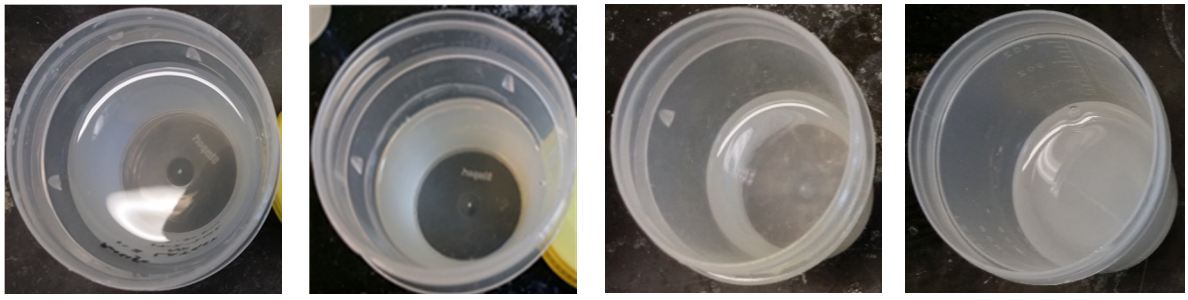

Figure 7. Pot-life of precursor solutions (**a**) TG and (**b**) LA(TG) after 30 days of preparation. (**c**) ST after 30 h of preparation and (**d**) LA(ST) after 17 h of preparation.

3.5. Impact of Low-VOC Content

Alcohol emissions from coatings contribute to the formation of greenhouse gases and are regulated as volatile organic compounds (VOCs) in the coatings industry. For the TGST coatings to conform to the low VOC requirement, alcohols formed as a by-product of hydrolysis of the precursors TG and ST were removed and replaced with deionized water to form the LA(TG) and LA(ST) solutions, which were then used to form the LA(TGST) crosslinked coatings with varying epoxide and thiol silicates stoichiometry (Scheme 1). The impact of the VOC content in the TGST systems to the environment was calculated using the ISO metric of Index of Global Warming Potential ($I_{(GWP)}$) [17] (Section 2.4, Equations (2) and (3)).

There are four hydrolysable ethoxy groups in TEOS that form ethanol in both the TG and the ST solutions and three hydrolysable methoxy groups in GPTMS and MPTMS forming methanol. Therefore, an equal stoichiometric amount of a mixture of ethanol and

methanol is emitted from the TG and the ST solutions. The $I_{(GWP)}$ for TG and ST solutions as prepared was calculated to be 45.57. $I_{(GWP)}$ values for the crosslinked TGST systems as prepared were calculated to be between 182.3 for the TGST 3:1 and 1:3 systems, 91.14 for the TGST 1:1 and 136.70 for the 2:1 and 1:2 TGST formulations. Therefore, the removal of alcohols from the LA(TGST) formulations reduces these impacts to global warming completely. In addition, a factor that contributes to the $I_{(GWP)}$ metric is the production of carbon dioxide from the use of fossil fuel as an energy source for heating during the evaporation of alcohols. For this work, $I_{(GWP)}$ due to heating the TG and ST formulations during the evaporation of alcohols was calculated [19] to be 0.25, which insignificantly diminishes the positive impact of LA(TGST) systems on $I_{(GWP)}$.

3.6. Coatings Performance

Performance of the LA(TGST) surface treatment coatings was evaluated using corrosion inhibition and scratch resistance tests. Corrosion inhibition of the coatings was tested by immersing coated steel coupons in Dilute Harrison's Solution (DHS), and scratch resistance was evaluated by pencil hardness tests following the ASTM D3363 standard. Similar tests were conducted on the TGST coatings for comparison.

3.6.1. Corrosion Inhibition

Low-carbon steel panels were dip-coated in the LA(TGST) or TGST formulations as described in Section 2.3 and air-dried for 24 h. Depending on the stoichiometry of the formulation, coated panels displayed varying degrees of a dark green layer that develops via an interaction between the thiol species and iron from the substrate potentially from the formation of the iron sulfates as presented in the XPS S2p analysis (Figure 4b,c).

Figure 8 shows pictures of the panels after 25 h of exposure to DHS for both the LA(TGST) and the TGST coatings systems. Figure 9 shows the calculated rust percentage of the scribed and unscribed panels at 24 h.

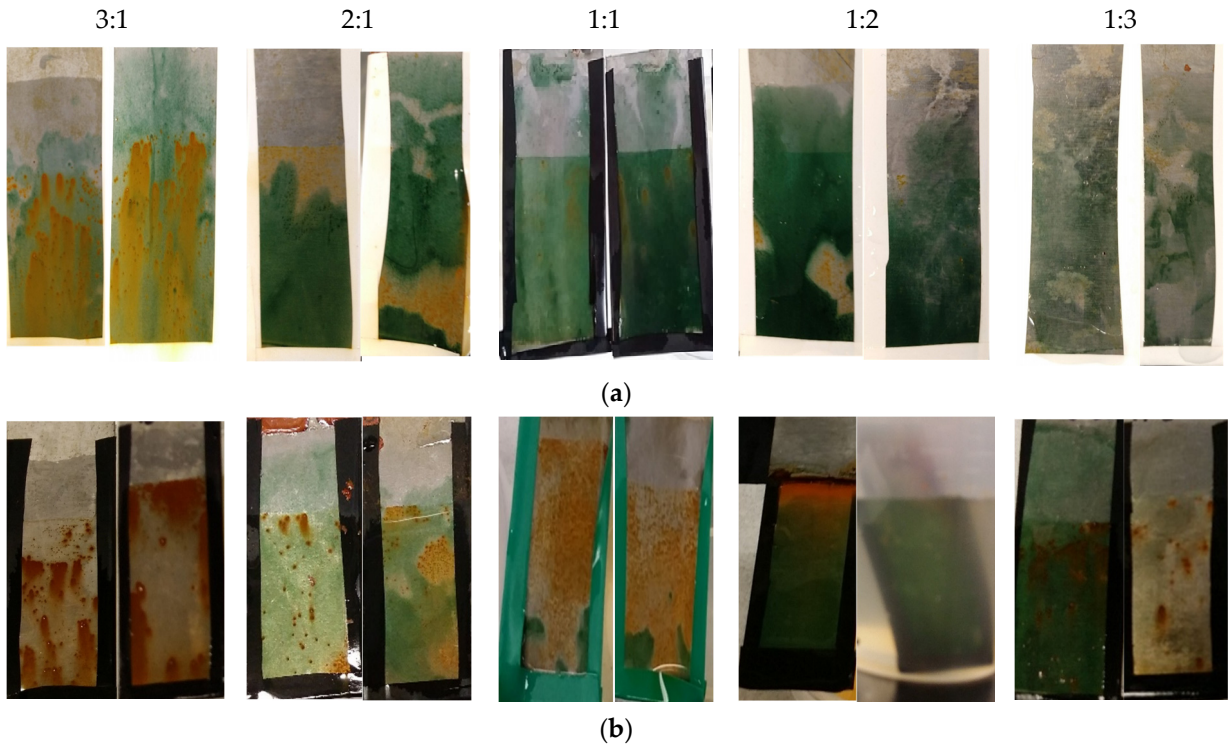

Figure 8. Corrosion prevention performance associated with development of rust on coupons coated with (**a**) TGST and (**b**) LA(TGST) formulations with varying TG:ST stoichiometry between 3:1 to 1:3 after exposure for 25 h in Dilute Harrison's Solution (DHS).

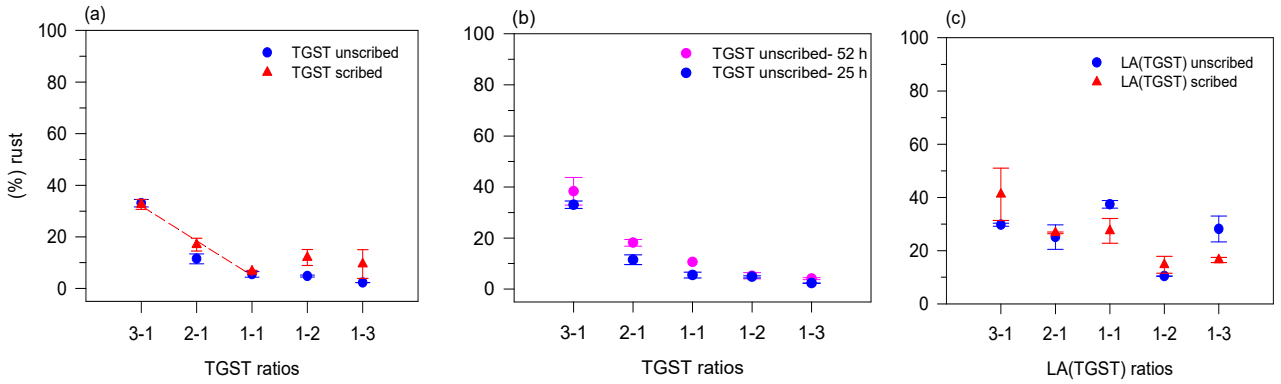

Figure 9. Rust percentage after exposure for the unscribed (●) and scribed (▲) panels (n = 3), coated with TGST and LA(TGST) in DHS. (**a**) TGST at 25 h, (**b**) comparison of unscribed TGST at 25 h and 52 h and (**c**) LA(TGST) at 25 h. The dashed red line in (**a**) is a guide for the eye.

From Figure 8, it is evident that the TGST coatings possess better corrosion inhibition properties than the low-alcohol LA(TGST) coatings for all TG:ST ratios. This clearly signifies that the removal of alcohols from the ST formulation affects the stability (Figure 7d) of the crosslinked LA(TGST) formulations and directly impacts the corrosion prevention performance of the coatings. This result introduced an area under investigation with promising results into a low-GWP impact LA(TG)ST system where the alcohols are removed only from the TG component of the formulation. It is of note that overall, the maximum corrosion for all crosslinked coatings did not exceed 40%, and the LA(TGST) coatings also performed better than the non-crosslinked TG and ST precursor formulations; TG-only formulations showed swelling and peeling at 1.5 h, and the ST-only coatings were between 60 and 80% corroded at 25 h [3]. TGST and LA(TGST) 3:1 coatings showed the earliest onset of corrosion (<3 h) and were extensively corroded at 25 h (Figure 8a,b), which was associated with the higher TG concentration and lowest crosslink density (Table 1, Figures 2d, 3c,d and 4c). In comparison, the TGST 1:1, 1:2, and 1:3 coatings with a higher ST concentration were substantially less corroded at 25 h (Figure 8a). This result corroborates the spectroscopic results obtained from Raman (Figure 2), FTIR (Figure 3), and XPS (Figure 4) analyses, confirming the direct positive impact of the higher thiol content and improved crosslinking on the corrosion resistance of coatings.

Coatings with higher epoxide ratios showed an early onset of corrosion and maximum rust formation associated with the higher concentration of the polar epoxide functional group in both the LA(TGST) and TGST systems (≈30% Figure 9a,c). LA(TG) and TG, which are epoxy decorated (Scheme 1), are also mildly susceptible to epoxide ring opening by water due to the presence of the acetic acid in the aqueous medium [36], although this process is slow for weak acids [37]. It could lead to an increase in hydroxyl groups in the formulation and therefore a decrease in corrosion resistance. Coatings with higher ST concentration showed better corrosion prevention properties in TGST (1:2 and 1:3, Figure 9a) due to the increased hydrophobicity attributed to the higher concentration of the relatively less polar thiol and disulfide groups (Figure 9a). Therefore, a linear scaling of corrosion inhibition matched by a linear decrease in rust percent would be expected for TG:ST stoichiometric ratios 1:1 to 1:3 due to increased hydrophobicity. Interestingly, corrosion inhibition improved with (i) decreasing TG content from 3:1 to 1:1 TGST, which is shown as a dashed red line in Figure 9a but showed no significant change between TGST 1:1 and 1:3 (Figure 9a). This surprisingly indicates that there is a diminishing difference between the increase in thiol content after TG:ST 1:1 and the onset of corrosion. The plateau after 1:1 TG:ST stoichiometry indicates that the crosslinking, hydrophobicity, and substrate–coating interactions at 1:1 TG:ST stoichiometry are sufficiently developed for protecting the substrate from the onset of corrosion. Although this would surprisingly indicate that an excess ST concentration promotes hydrophobicity, improved crosslinking, including

disulfide dimerization and a more expanded siloxane network, would be redundant for corrosion protection; Figure 9b demonstrates that improved crosslinking assists in sustaining the protection under prolonged exposure. At 52 h of immersion in the salt solution, the rust percentage increases for TGST 1:1 but remains practically unchanged in TGST 1:2 and 1:3. It is also of note that only a 2–6% increase in rust is observed between 25 and 52 h of exposure (Figure 9b) and despite the doubled exposure time, the overall rust percentage is maintained below 40%, even in the most corroded TGST 3:1 coating.

It is also telling that the 3:1 and 2:1 ratios of the LA(TGST) system (Figure 9c) have comparable rust percentage as the corresponding TGST coatings (Figure 9a); however, a large fluctuation in the rust percentage values of 1:1, 1:2, and 1:3 LA(TGST) coatings is observed. In coatings where the LA(TG) concentration is high, the formulation is relatively stable in the absence of alcohols, and corrosion resistance, although limited, is consistent (Figure 6, TGST and LA(TGST) 3:1 and 2:1 Figure 9a,c). In coatings where the LA(ST) concentration is high, the elimination of alcohols causes the formulation to be less stable and corrosion resistance to be poor (Figures 6b and 7d, LA(TGST) 1:2 and 1:3, Figure 9c). Although the formation of rust in the ratios with higher LA(ST) concentration appears to be random, LA(TGST) 1:2 has the best corrosion resistance performance compared to LA(TGST) 1:1 and 1:3 (Figure 9c). These results agree with the results from FTIR (Figure 3) that show that the same amount of LA(TG) is consumed for crosslinking by LA(ST) at all ratios irrespective of LA(TG):LA(ST) stoichiometry; therefore, any corrosion protection in this system is contributed by disulfide hydrophobicity and not epoxy–thiol crosslinking density. Although all LA(TGST) coatings had exhibited extensive corrosion at 25 h (Figure 8b), the LA(TGST) 1:2 ratio showed the maximum corrosion protection in the series. Overall, the corrosion prevention results demonstrated that TGST 1:1 to 1:3 showed between 96% and 97% improvement in corrosion inhibition over the non-crosslinked formulations, and even the most corroded LA(TGST) formulations exhibited a 71% improvement in protection.

3.6.2. Pencil Hardness

All coatings were glossy, homogenously coated, and showed a layer of green depending on the ratio of formulation. The surface hardness and scratch resistance of all hybrid coatings associated with extent of cure were evaluated with the pencil hardness test. The process was started with the hardest pencil, number 9H by rolling it on the surface of each coating following the procedure recommended by the ASTM standard. The procedure was repeated with pencils of all hardnesses on the test scale. It is of note that none of the pencils, including the hardest 9H pencil, did not scratch or gouge the surface of any coating, maintaining both the integrity and the gloss of the surface of the coatings. This result confirms that the coatings from all formulations were extensively cured and possessed high-scratch resistance properties across all ratios.

4. Conclusions

Environmentally sustainable, epoxy–thiol silicate crosslinked coatings with low volatile organic content (VOC) were prepared to investigate the impact of elimination of alcohols on the extent of epoxy–thiol and sol–gel silicate network crosslinking density. Two series of waterborne formulations with varying epoxy–thiol silicate stoichiometry from 3:1 to 1:3 were synthesized. In the first series, alcohols (methanol and ethanol) that are the by-product of the sol–gel reactions were removed from the precursors to prepare low-alcohol (LA) epoxy silicate (TG) and thiol silicate (ST) crosslinked hybrid coatings (LA(TGST)). A second series (TGST), where alcohols were retained, was synthesized in similar ratios to compare the impact of alcohols on the crosslinking density, formulation stability, viscosity, pot-life, and corrosion-prevention performance of the coatings. The positive impact on the environment by the elimination of VOCs from LA(TGST) coatings was quantified using ISO metrics for global warming potential (GWP). A significant improvement in GWP was offset by colloidal instability in most of the low-alcohol formulations with higher LA(ST) content. Raman and FTIR spectroscopy indicated that all formulations showed successful

crosslinking of functional groups, and the structural integrity of the low-alcohol formulations was sustained even in the absence of alcohols. Curing was at its maximum after 17 h of crosslinking time and depended on thiol concentration. It was expected that a variation in the thiol concentration would increase the accessibility of these groups to complement crosslinking mechanisms with epoxy functional groups and further enhance the corrosion resistance properties. Spectroscopic evidence by Raman, FTIR, and XPS spectroscopies confirmed an increase in epoxy–thiol crosslinking density and hydrophobicity due to disulfide dimerization that contributed to maximizing corrosion protection. However, formulation stability associated with viscosity and pot-life was found to be a function of both crosslinking density between the functional groups and the presence of alcohols in the system. It was established that the corrosion prevention performance of coatings for the low-alcohol system was directly related to the increased hydrophobicity of the sulfur moiety rather than the epoxy–thiol crosslinking density. Both LA(TGST) and TGST systems showed enhanced corrosion prevention compared to the non-crosslinked TG and ST formulations and contained corrosion below 40% even in the most corroded samples. The 1:1 TGST stoichiometry was found to be sufficiently crosslinked and hydrophobic to provide maximum corrosion inhibition compared to the other ratios, but the improved crosslinking density in 1:2 and 1:3 TGST was evidenced to provide sustained protection even when the coatings were exposed to double the exposure time in a corrosive environment. In the low-alcohol series, the LA(TG):LA(ST) ratio 1:2 showed the most effective corrosion inhibition and overall performed 71% better than the non-crosslinked hybrids. Glossy, scratch-resistant thin film coatings with enhanced corrosion inhibition for surface treatment of low-carbon steel were successfully achieved. Pot-life, ease of smooth coating, and corrosion inhibition data indicated that the formulations are suitable for industrial applications as a primer in the marine coatings industry.

Supplementary Materials: The following are available online at https://www.mdpi.com/2079-6412/11/3/306/s1, Figure S1: Structural characterization the hybrid (a) TGST and (b) low-alcohol LA(TGST) formulations FTIR spectroscopy in the fingerprint region for all TG:ST ratios, Figure S2: Raman spectra showing the variation of epoxy and thiol peaks for reaction of TGST at 17 h, Figure S3: Pot-life for TGST solutions at different crosslinking times (a) t = 0 h, (b) t = 20 h, Figure S4: Pot-life for LA(TGST) solutions at crosslinking times t = 20 h.

Author Contributions: S.S.: Conceptualization, writing, editing, data curation, formal analysis, investigation, methodology, software, validation, literature research, visualization, chemical schemes/figures/tables. A.J.V.: Editing, Resources. O.S.: XPS data analysis. All authors have read and agreed to the published version of the manuscript.

Funding: This research received no external funding.

Conflicts of Interest: The authors declare no conflict of interest.

References

1. Innocenzi, P. Understanding sol–gel transition through a picture. A short tutorial. *J. Sol-Gel Sci. Technol.* **2020**, *94*, 544–550. [CrossRef]
2. Kappert, E.J.; Pavlenko, D.; Malzbender, J.; Nijmeijer, A.; Benes, N.E.; Tsai, P.A. Formation and prevention of fractures in sol–gel-derived thin films. *Soft Matter* **2015**, *11*, 882–888. [CrossRef] [PubMed]
3. Shetranjiwalla, S.; Vreugdenhil, A.; Stotesbury, T. Waterborne epoxy-thiol decorated silica sol-gel coatings: Impact of crosslinking on corrosion prevention. *J. Sol-Gel Sci. Technol.* **2018**, *87*, 504–513. [CrossRef]
4. Guin, A.K.; Bhadu, M.; Sinhababu, M.; Udayabhanu, G. The effect of zirconia ions on corrosion performance of sol–gel coated galvanized steel. *J. Coat. Technol.* **2014**, *11*, 967–977. [CrossRef]
5. Al-Sagheer, F.; Merchant, S. Visco-elastic properties of chitosan–titania nano-composites. *Carbohydr. Polym.* **2011**, *85*, 356–362. [CrossRef]
6. Lu, X.; Hasegawa, G.; Kanamori, K.; Nakanishi, K. Hierarchically porous monoliths prepared via sol–gel process accompanied by spinodal decomposition. *J. Sol-Gel Sci. Technol.* **2020**, *95*, 530–550. [CrossRef]
7. Brinker, C.J.; Scherer, G.W. *Sol-Gel Science: The Physics and Chemistry of Sol-Gel Processing*; Academic Press: Cambridge, MA, USA, 2013.
8. Bera, S.; Rout, T.; Udayabhanu, G.; Narayan, R. Comparative study of corrosion protection of sol–gel coatings with different organic functionality on Al-2024 substrate. *Prog. Organ. Coat.* **2015**, *88*, 293–303. [CrossRef]

9. Guin, A.K.; Nayak, S.; Rout, T.; Bandyopadhyay, N.; Sengupta, D. Corrosion behavior of nanohybrid titania–silica composite coating on phosphated steel sheet. *J. Coat. Technol. Res.* **2012**, *9*, 97–106. [CrossRef]
10. Malay, O.; Yilgor, I.; Menceloglu, Y.Z. Effects of solvent on TEOS hydrolysis kinetics and silica particle size under basic conditions. *J. Sol-Gel Sci. Technol.* **2013**, *67*, 351–361. [CrossRef]
11. Serra, A.; Ramis, X.; Fernández-Francos, X. Epoxy sol-gel hybrid thermosets. *Coatings* **2016**, *6*, 8. [CrossRef]
12. Li, G.; Wang, X.; Li, A.; Wang, W.; Zheng, L. Fabrication and adhesive properties of thin organosilane films coated on low carbon steel substrates. *Surf. Coat. Technol.* **2007**, *201*, 9571–9578. [CrossRef]
13. Bera, S.; Rout, T.; Udayabhanu, G.; Narayan, R. Water-based & eco-friendly epoxy-silane hybrid coating for enhanced corrosion protection & adhesion on galvanized steel. *Prog. Organ. Coat.* **2016**, *101*, 24–44.
14. Vreugdenhil, A.; Balbyshev, V.; Donley, M. Nanostructured silicon sol-gel surface treatments for Al 2024-T3 protection. *J. Coat. Technol.* **2001**, *73*, 35–43. [CrossRef]
15. Beccaria, A.M.; Padeletti, G.; Montesperelli, G.; Chiaruttini, L. The effect of pretreatments with siloxanes on the corrosion resistance of aluminium in NaCl solution. *Surf. Coat. Technol.* **1999**, *111*, 240–246. [CrossRef]
16. Rueden, C.T.; Schindelin, J.; Hiner, M.C.; DeZonia, B.E.; Walter, A.E.; Arena, E.T.; Eliceiri, K.W. ImageJ2: ImageJ for the next generation of scientific image data. *BMC Bioinform.* **2017**, *18*, 529. [CrossRef] [PubMed]
17. Guinée, J.B.; Lindeijer, E. *Handbook on Life Cycle Assessment: Operational Guide to the ISO Standards*; Springer Science & Business Media: Berlin/Heidelberg, Germany, 2002; Volume 7.
18. Allen, D.T.; Shonnard, D.R. *Green Engineering: Environmentally Conscious Design of Chemical Processes*; Pearson Education: New York, NY, USA, 2001.
19. Mooney, M.; Vreugdenhil, A.J.; Shetranjiwalla, S. A Toolkit of Green Chemistry and Life-Cycle Analysis for Comparative Assessment in Undergraduate Organic Chemistry Experiments: Synthesis of (E)-Stilbene. *J. Chem. Educ.* **2020**, *97*, 1336–1344. [CrossRef]
20. Petrie, E.M. *Epoxy Adhesive Formulations*; McGraw Hill Professional: Pennsylvania, NY, USA, 2005.
21. Bera, S.; Udayabhanu, G.; Narayan, R.; Rout, T. High performance chrome free coating for white rust protection of zinc. *Mater. Sci. Technol.* **2016**, *32*, 338–347. [CrossRef]
22. Zheng, S.; Li, J. Inorganic–organic sol gel hybrid coatings for corrosion protection of metals. *J. Sol-Gel Sci. Technol.* **2010**, *54*, 174–187. [CrossRef]
23. Lin-Vien, D.; Colthup, N.B.; Fateley, W.G.; Grasselli, J.G. *The Handbook of Infrared and Raman Characteristic Frequencies of Organic Molecules*; Elsevier: Amsterdam, The Netherlands, 1991.
24. Launer, P.; Arkles, B. *Silicon Compounds: Silanes & Silicones*; Gelest Inc.: Morrisville, PA, USA, 2013.
25. Coates, J. *Interpretation of Infrared Spectra, a Practical Approach*; Meyers, R.A., Ed.; John Wiley & Sons Ltd.: Chichester, UK, 2000.
26. Beamson, G.; Briggs, D. High resolution monochromated X-ray photoelectron spectroscopy of organic polymers: A comparison between solid state data for organic polymers and gas phase data for small molecules. *Mol. Phys.* **1992**, *76*, 919–936. [CrossRef]
27. Johnson, B.I.; Avval, T.G.; Wheeler, J.; Anderson, H.C.; Diwan, A.; Stowers, K.J.; Ess, D.H.; Linford, M.R. Semiempirical Peak Fitting Guided by ab Initio Calculations of X-ray Photoelectron Spectroscopy Narrow Scans of Chemisorbed, Fluorinated Silanes. *Langmuir* **2020**, *36*, 1878–1886. [CrossRef]
28. Laibinis, P.E.; Whitesides, G.M.; Allara, D.L.; Tao, Y.T.; Parikh, A.N.; Nuzzo, R.G. Comparison of the structures and wetting properties of self-assembled monolayers of n-alkanethiols on the coinage metal surfaces, copper, silver, and gold. *J. Am. Chem. Soc.* **1991**, *113*, 7152–7167. [CrossRef]
29. Nesbitt, H.; Bancroft, G.; Pratt, A.; Scaini, M. Sulfur and iron surface states on fractured pyrite surfaces. *Am. Mineral.* **1998**, *83*, 1067–1076. [CrossRef]
30. Bain, C.D.; Biebuyck, H.A.; Whitesides, G.M. Comparison of self-assembled monolayers on gold: Coadsorption of thiols and disulfides. *Langmuir* **1989**, *5*, 723–727. [CrossRef]
31. Morf, P.; Raimondi, F.; Nothofer, H.-G.; Schnyder, B.; Yasuda, A.; Wessels, J.M.; Jung, T.A. Dithiocarbamates: Functional and versatile linkers for the formation of self-assembled monolayers. *Langmuir* **2006**, *22*, 658–663. [CrossRef]
32. Castner, D.G.; Hinds, K.; Grainger, D.W. X-ray photoelectron spectroscopy sulfur 2p study of organic thiol and disulfide binding interactions with gold surfaces. *Langmuir* **1996**, *12*, 5083–5086. [CrossRef]
33. Terzyk, A.P. The influence of activated carbon surface chemical composition on the adsorption of acetaminophen (paracetamol) in vitro: Part II. TG, FTIR, and XPS analysis of carbons and the temperature dependence of adsorption kinetics at the neutral pH. *J. Colloids Surf. A Physicochem. Eng. Asp.* **2001**, *177*, 23–45. [CrossRef]
34. Wu, T.; Xu, J.; Yan, M.; Sun, C.; Yu, C.; Ke, W. Synergistic effect of sulfate-reducing bacteria and elastic stress on corrosion of X80 steel in soil solution. *Corros. Sci.* **2014**, *83*, 38–47. [CrossRef]
35. Bagiyan, G.; Koroleva, I.; Soroka, N.; Ufimtsev, A.V. Oxidation of thiol compounds by molecular oxygen in aqueous solutions. *Russ. Chem. Bull.* **2003**, *52*, 1135–1141. [CrossRef]
36. Hoebbel, D.; Nacken, M.; Schmidt, H. A NMR Study on the Hydrolysis, Condensation and Epoxide Ring-Opening Reaction in Sols and Gels of the System Glycidoxypropyltrimethoxysilane-Water-Titaniumtetraethoxide. *J. Sol-Gel Sci. Technol.* **1998**, *12*, 169–179. [CrossRef]
37. Vreugdenhil, A.; Horton, J.; Woods, M. Fabrication, characterization and modification of nanodimensional silica hybrid multilayered materials. *J. Non-Cryst. Solids* **2009**, *355*, 1206–1211. [CrossRef]